



## OPEN ACCESS

## EDITED BY

Muhammad Mubashir Bhatti,  
Shandong University of Science and  
Technology, China

## REVIEWED BY

Abayomi Samuel Oke,  
Adekunle Ajasin University, Nigeria  
H. A. Kumara Swamy,  
Presidency University, India  
N. Keerthi Reddy,  
Ulsan National Institute of Science and  
Technology, South Korea  
Muhammad Bilal Arain,  
International Islamic University, Pakistan  
Puneet Rana,  
Wenzhou University, China  
Ebenezer Bonyah,  
University of Education, Winneba, Ghana

## \*CORRESPONDENCE

Pramet Kaewmesri,  
pramet.kae@gistda.or.th

## SPECIALTY SECTION

This article was submitted to  
Interdisciplinary Physics,  
a section of the journal  
Frontiers in Physics

RECEIVED 07 July 2022

ACCEPTED 26 July 2022

PUBLISHED 20 October 2022

## CITATION

Wakif A, Abderrahmane A, Guedri K,  
Bouallegue B, Kaewthongrach R,  
Kaewmesri P and Jirawattanapanit A  
(2022), Importance of exponentially  
falling variability in heat generation on  
chemically reactive von Kármán  
nanofluid flows subjected to a radial  
magnetic field and controlled locally by  
zero mass flux and convective heating  
conditions: A differential  
quadrature analysis.  
*Front. Phys.* 10:988275.  
doi: 10.3389/fphy.2022.988275

## COPYRIGHT

© 2022 Wakif, Abderrahmane, Guedri,  
Bouallegue, Kaewthongrach,  
Kaewmesri and Jirawattanapanit. This is  
an open-access article distributed under  
the terms of the [Creative Commons  
Attribution License \(CC BY\)](https://creativecommons.org/licenses/by/4.0/). The use,  
distribution or reproduction in other forums  
is permitted, provided the original author(s)  
and the copyright owner(s) are credited and  
that the original publication in this journal is  
cited, in accordance with accepted  
academic practice. No use, distribution or  
reproduction is permitted which does not  
comply with these terms.

# Importance of exponentially falling variability in heat generation on chemically reactive von Kármán nanofluid flows subjected to a radial magnetic field and controlled locally by zero mass flux and convective heating conditions: A differential quadrature analysis

Abderrahim Wakif<sup>1</sup>, Aissa Abderrahmane<sup>2</sup>, Kamel Guedri<sup>3</sup>,  
Belgacem Bouallegue<sup>4,5</sup>, Rungrapa Kaewthongrach<sup>6</sup>,  
Pramet Kaewmesri<sup>7\*</sup> and Anuwat Jirawattanapanit<sup>8</sup>

<sup>1</sup>Laboratory of Mechanics, Faculty of Sciences Ain Chock, Hassan II University of Casablanca, Casablanca, Morocco, <sup>2</sup>LPQ3M, Université Mustapha Stambouli de Mascara, Mascara, Algeria, <sup>3</sup>Mechanical Engineering Department, College of Engineering and Islamic Architecture, Umm Al-Qura University, Makkah, Saudi Arabia, <sup>4</sup>College of Computer Science, King Khalid University, Abha, Saudi Arabia, <sup>5</sup>Electronics and Micro-Electronics Laboratory (E. μ. E. L), Faculty of Sciences of Monastir, University of Monastir, Monastir, Tunisia, <sup>6</sup>Geo-Informatics and Space Technology Development Agency (GISTDA), Chonburi, Thailand, <sup>7</sup>Geo-Informatics and Space Technology Development Agency (GISTDA), Bangkok, Thailand, <sup>8</sup>Department of Mathematics, Faculty of Science, Phuket Rajabhat University (PKRU), Phuket, Thailand

Owing to the various physical aspects of nanofluids as thermally enhanced working fluids and the significance of swirling flows in rheological devices as well as in the spin coating and lubrication applications, the current comprehensive examination aimed to explore the important features of spinning flows of chemically reactive Newtonian nanofluids over a uniformly revolving disk in the existence of a radially applied magnetic field along with an exponentially decaying space-dependent heat source, in the case where the disk surface is heated convectively and unaffected by the vertical nanoparticles' mass flux. Based on feasible boundary layer approximations and Buongiorno's nanofluid formulation, the leading coupled differential equations are stated properly in the sense of Arrhenius's and Von Kármán's approaches. By employing an advanced generalized differential quadrature algorithm, the obtained boundary layer equations are handled numerically with a higher order of accuracy to generate adequate graphical and tabular illustrations for the different values of the influencing flow parameters. As findings, the graphical results confirm that the nanofluid motion decelerates meaningfully thanks to the resistive magnetic influence. A significant thermal amelioration can be achieved by strengthening the magnetic impact, the generation of heat, the thermal convective process, and the thermophoresis

mechanism. Moreover, it is found that the thermo-migration of nanoparticles can be reinforced more *via* the intensification in the convective process, the thermo-migration of nanoparticles, and the activation energy.

#### KEYWORDS

enhanced swirling nanofluid flow, non-homogeneous model, radial magnetic field, arrhenius kinetics, zero mass flux condition

## 1 Introduction

During the last decades, the topic of heat/mass enhancement through multi-phase flows (e.g., monotype/hybrid/ternary nanofluid flows) has attracted amazing consideration from the scientific communities around the globe owing to their widespread necessity in several practical domains (e.g., the ameliorating the combustion characteristics of diesel fuel in compression ignition engines). In this context, it was demonstrated through a benchmark experimental investigation [1] and other authenticated sources [2, 3] that regular liquids (e.g., oil, ethylene glycol, and water) are not preferred thermally as working fluids due to their weak thermal conductance. As technical propositions, it was advised that the insertion of tiny/nano-sized particles (e.g., alumina, graphene, copper oxide, gold, titania, silver, copper, as well as single- and multi-walled carbon nanotubes) is among the best feasible way for improving the thermal performances of pure fluids on the condition that the adding solid nanoparticles should have a higher thermal conductivity as compared with the host fluid. Such a biphasic mixture (i.e., nanoparticles and base fluid) was named a nanofluid for the first time in 1995 by Choi and Eastman [4]. Thanks to the latest progress in the mixture theory and the science therein, the existing experimental and theoretical literature surveys involve an exhaustive overview regarding the principal specific appearances describing persuasively the physical, thermal, and rheological aspects of nanofluids [5–10]. In this respect, it was reported that the thermophysical proprieties of nanofluids depend on several influential factors (e.g., shape/size of nanoparticles as well as their concentration and temperature) that can affect significantly the heat transfer within a nanofluidic medium and its flow pattern. By linking theoretically the bioconvection occurrence phenomenon to other thermal and mass transport processes, Waqas et al. [11] proposed advanced non-homogeneous flow models constrained by realistic physical impacts to explore the consequence of swimming motile microorganisms on the hydrothermal and mass features of slippery nanofluid flows near a variable thick surface of a rotating disk. More recently, Shah et al. [12] exploited the possibility of hybridizing the nanoparticles *MWCNT* and  $Fe_3O_4$  in a suitable base fluid to examine thermodynamically the behavior of a magnetized hybrid nanofluid inside a porous cavity structure in the presence of a tilted magnetic field. The same solid mixture was employed also by Maneengam et al. [13] in pure water to study the irreversibility

features and MHD flow patterns of the hybrid nanofluid ( $Fe_3O_4 + MWCNT$ ) –  $H_2O$  inside a lid-driven corrugated porous cavity. Further hydrothermal and entropic appearances of the nanofluid  $Al_2O_3 - H_2O$  were evidenced comprehensively by Alshare et al. [14] during its MHD natural convective motion inside a lid-driven wavy cavity with an elliptical obstacle by employing a robust numerical code based on the Galerkin weighted residual finite element technique.

Convective flows over rotating heated disk-shaped bodies are considered among the main popular dynamical problems treated fundamentally in fluid mechanics and heat transfer since a long time ago. Further, the dealing of flows near rotating disks is of great interest to the majority of researchers not only for comprehending the occurring flow regimes but also for their diverse uses (e.g., stability control of swirling flows, domestic devices, rotating heat exchangers, visco-rheometers, chemical stirring operations, spinning disk reactors, vehicle engines, and productive aero-hydrodynamic turbines). In this respect, several examinations were accomplished roughly for such flow problems [15–17]. In 1921, Von Kármán [18] was the first pioneering scientist who discussed theoretically the dynamical axisymmetric aspect of steady swirling flows driven over a rotating infinite disk for incompressible viscous fluids. Based on the boundary layer theory, Navier-Stokes's mathematical formulation of this famous fluid flow problem can be extended reasonably to the case of non-Newtonian fluids [19, 20] (e.g., Bingham and tangent hyperbolic fluid models). Mathematically, the simplified boundary layer equations can be reduced to a nonlinear system of coupled ordinary differential equations, whose similar solutions can be derived semi-analytically or numerically through the modified so-called Von Kármán's integral momentum equation. Keeping in mind the rheological and thermal importance of nanofluids and their applicabilities in Von Kármán's flow configuration, several scrutinizations were performed recently on nanofluid flows over a rotating disk. In this context, Waini et al. [21] performed a numerical stability analysis of unsteady axisymmetric swirling flows of  $(Al_2O_3 + Cu) - H_2O$  hybrid nanofluids over an isothermally heated disk. By utilizing the same hybrid mixture, Kumar et al. [22] invoked the entropy minimization approach along with Von Kármán's strategy to quantify the different thermodynamical irreversibilities that can be happened during the radiative magnetohydrodynamic slipping flows of  $(Al_2O_3 + Cu) - H_2O$  hybrid nanofluids over a rotating heated disk when the strengths of Ohmic heating and viscous dissipation are significant. Similarly, Mandal and Shit [23] assumed the effective contribution of non-Newtonian viscous dissipation and Joule heating to carry out a numerical entropic scrutinization on unsteady axisymmetric MHD flows of radiative Casson nanofluids over a turning permeable disk,

which was supposed to be heated convectively, stretched radially, and embedded horizontally in a quiescent nanofluidic medium containing ethylene glycol or water as a holding fluid and alumina or copper as nanoparticles. From another strategical point of view, Magodora et al. [24] preferred employing the non-homogeneous nanofluid model of Buongiorno [25] to show the significance of Brownian and thermophoresis diffusions of nanoparticles on the onset of heat and mass transport during the axisymmetric swirling motion of a chemically reacting nanofluid containing water and gold nanomaterials nanofluid near a rotating heated disk. In another multi-diffusive problem, Latiff et al. [26] considered Stefan's blowing influence and bioconvection occurrence to examine the hydrothermal appearances along with the resulting mass transport phenomena during the unsteady nanofluid motion over a spinning stretchable disk.

Nonetheless, inclusive studies on the significant impacts of Arrhenius's chemical reactive kinetics, the thermo-migration diffusive process, and the Brownian motion of nanoparticles on MHD Von Kármán non-homogeneous flows of chemically reacting nanofluids over a horizontal turning disk are still rare in the available literature, in the case of zero mass flux and thermal convective conditions, and especially when the electrically conducting nanofluidic medium is exposed to an adjustable magnetic source acting radially, which is enhanced thermally *via* an exponentially decaying space-dependent heat source. Motivated by this pending scientific concern, the present examination aimed surely to provide definitive answers on this open topic. Accordingly, an appropriate MHD nanofluid flow model has been developed properly in this regard by adopting the renovated version of Buongiorno's approach. Based on the generalized boundary layer simplifications and other admissible physical assumptions, the leading conservation equations are derived mathematically in the form of coupled partial differential equations (PDEs) together with their corresponding realistic boundary conditions (BCs), which are rewritten thereafter as a set of strongly nonlinear ordinary differential equations (ODEs) having no closed-form solutions. For this reason, an advanced hybrid algorithm has been implemented numerically in Matlab software. After performing extensive validating tests, the generated datasets are presented skillfully to provide a comprehensive physical discussion through the following research questions:

- 1- How can formulate a proper MHD non-homogeneous Von Kármán flow model for a chemically reactive nanofluid by considering the effective contribution of Brownian and thermophoresis diffusions and utilizing the molar concentration notion, in the case where the external magnetic field is exerted radially in the presence of an exponentially decaying heat generation?
- 2- How can associate the generalized differential quadrature algorithm with Newton-Raphson's technique in a methodological solution to evidence the present three-dimensional MHD convective nanofluid motion and determine the temperature and nanoparticles' molar concentration distributions?
- 3- What are the advantages of using GDQM- NRIT as a hybrid numerical approach?
- 4- When and to what computational level we can consider that the outputted results are numerically admissible?
- 5- What are the dynamical and thermal impacts of the applied external magnetic field?
- 6- Which control parameters can exhibit an enhancing thermal trend?
- 7- How can determine the unknown wall characteristics related to the nanoparticles' molar concentration and the temperature by exploiting the conditions of zero mass flux and convective heating?
- 8- What are the mass influences of convective heating and Arrhenius's chemical reaction on the Brownian and thermophoretic migrations of nanoparticles?

## 2 Governing equations and physical model

Let's consider a steady laminar nanofluid flow over an impermeable disk of infinite extension, which is rotated uniformly around its symmetrical  $z$ -axis with an angular velocity  $\Omega$  and heated convectively thanks to a surrounding hot working fluid of temperature  $T_f$ . As an additional presumption, a destructive reactive process is taken place chemically throughout the Newtonian nanofluidic medium according to Arrhenius's kinetics. Initially, the geometrical configuration is positioned horizontally in a quiescent nanofluidic medium, which is featured physically by the pressure  $p_\infty$ , the temperature  $T_\infty$ , and the nanoparticles' molar concentration  $\chi_\infty$  as schematized tri-dimensionally in Figure 1. For a better description of the proposed nanofluid model, an appropriate cylindrical frame is chosen herein to provide a proper mathematical formulation in the cylindrical coordinate system  $(r, \phi, z)$ . Moreover, the convective swirling nanofluid motion has happened spatially nearby to a magnetic source applying radially a uniform magnetic field of intensity  $B$  in the presence of an exponentially decaying space-dependent thermal source. Furthermore, the wall characteristics  $(T_w, \chi_w)$  corresponding to the nanofluid temperature and nanoparticles' molar concentration at the contact surface are unknown as boundary conditions. However, their approximate values can be estimated computationally through the gradient expressions of the thermal and concentration boundary conditions (i.e., the convective heating and zero vertical mass flux conditions). For reducing the complexity of the nanofluid flow problem under consideration, the following physical presumptions are taken into account:

- The viscous nanofluid has a Newtonian rheological trend and behaves as a weakly electrically conducting medium, in which the induced magnetic field can be ignored in front of the externally applied magnetic field.

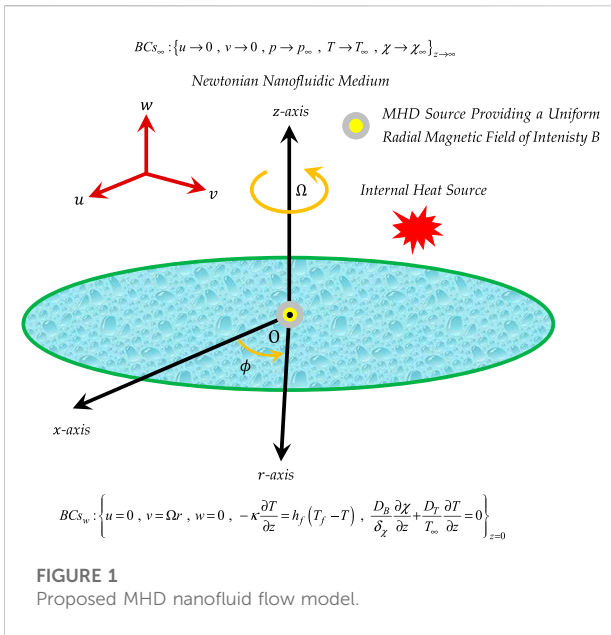


FIGURE 1 Proposed MHD nanofluid flow model.

- Since the strength of the applied magnetic field is not strong enough, the physical influence of Hall's current can be neglected obviously.
- In addition to the convective heating process and the existence of solid nanoparticles within the viscous nanofluidic medium, the occurred boundary layer regions are due also to the uniform rotation of the geometrical configuration.
- The momentum, thermal, and concentration boundary layer approximations are adopted along with the renewed Buongiorno's model to formulate the proposed nanofluid flow model.

- The governing PDEs of thermal energy and nanoparticles' distribution are adjusted appropriately by utilizing the molar concentration of nanoparticles  $\chi$  instead of their volume fraction  $\phi$ , where  $\chi = \delta_\chi \phi$ .
- The contribution of Brownian motion and thermophoresis mechanism are incorporated effectively in the proposed nanofluid flow model by invoking the two-phase nanofluid model.
- The base fluid is in local thermal equilibrium with the solid nanomaterials.

Based on the above statements, the leading conservation PDEs are written as:

$$\frac{\partial u}{\partial r} + \frac{u}{r} + \frac{\partial w}{\partial z} = 0, \tag{1}$$

$$u \frac{\partial u}{\partial r} - \frac{v^2}{r} + w \frac{\partial u}{\partial z} = -\frac{1}{\rho} \frac{\partial p}{\partial r} + v \left( \frac{\partial^2 u}{\partial r^2} + \frac{1}{r} \frac{\partial u}{\partial r} - \frac{u}{r^2} + \frac{\partial^2 u}{\partial z^2} \right), \tag{2}$$

$$u \frac{\partial v}{\partial r} + \frac{uv}{r} + w \frac{\partial v}{\partial z} = v \left( \frac{\partial^2 v}{\partial r^2} + \frac{1}{r} \frac{\partial v}{\partial r} - \frac{v}{r^2} + \frac{\partial^2 v}{\partial z^2} \right) - \frac{\sigma B^2}{\rho} v, \tag{3}$$

$$u \frac{\partial w}{\partial r} + w \frac{\partial w}{\partial z} = -\frac{1}{\rho} \frac{\partial p}{\partial z} + v \left( \frac{\partial^2 w}{\partial r^2} + \frac{1}{r} \frac{\partial w}{\partial r} + \frac{\partial^2 w}{\partial z^2} \right) - \frac{\sigma B^2}{\rho} w, \tag{4}$$

$$u \frac{\partial T}{\partial r} + w \frac{\partial T}{\partial z} = \left\{ \begin{aligned} & \frac{\kappa}{(\rho C_p)} \left( \frac{\partial^2 T}{\partial r^2} + \frac{1}{r} \frac{\partial T}{\partial r} + \frac{\partial^2 T}{\partial z^2} \right) + \frac{(\rho C_p)_{np} D_B}{(\rho C_p) \delta_\chi} \left( \frac{\partial T}{\partial r} \frac{\partial \chi}{\partial r} + \frac{\partial T}{\partial z} \frac{\partial \chi}{\partial z} \right) + \\ & \frac{(\rho C_p)_{np} D_T}{(\rho C_p) T_\infty} \left[ \left( \frac{\partial T}{\partial r} \right)^2 + \left( \frac{\partial T}{\partial z} \right)^2 \right] + \frac{Q(T_f - T_\infty)}{(\rho C_p)} e^{-\delta \sqrt{q} z} \end{aligned} \right\}, \tag{5}$$

$$u \frac{\partial \chi}{\partial r} + w \frac{\partial \chi}{\partial z} = \left( \frac{\partial^2}{\partial r^2} + \frac{1}{r} \frac{\partial}{\partial r} + \frac{\partial^2}{\partial z^2} \right) \left( D_B \chi + \frac{\delta_\chi D_T}{T_\infty} T \right) - K_\chi \left( \frac{T}{T_\infty} \right)^n (\chi - \chi_\infty) e^{-\frac{E_A}{K_B T}}. \tag{6}$$

TABLE 1 Pertinent flow parameters and their characteristics.

Parameters	Symbols/expressions	Default values	Ranges
Reynolds number	$Re_r = \frac{\Omega r^2}{\nu}$	-----	-----
Prandtl number	$Pr = \frac{\nu(\rho C_p)}{\kappa}$	3	Unchanged
Exponentially decaying parameter	$\delta$	1	Unchanged
Fitted rate constant	$n$	0.5	Unchanged
Temperature difference parameter	$\omega = \frac{T_f - T_\infty}{T_\infty}$	0.2	Unchanged
Chemical reaction parameter	$\Gamma = \frac{K_\chi}{\Omega}$	1	Unchanged
Magnetic parameter	$M = \frac{\sigma B^2}{\Omega \rho}$	1	$1 \leq M \leq 3$
Heat generation parameter	$Q_E = \frac{\nu Q}{\kappa \Omega}$	0.1	$0.1 \leq Q_E \leq 0.3$
Thermal Biot number	$Bi = \frac{h_f}{\kappa} \sqrt{\frac{\pi}{\Omega}}$	5	$1 \leq Bi \leq 5$
Thermophoresis parameter	$N_T = \frac{(\rho C_p)_{np} D_T \omega}{(\rho C_p) \nu}$	0.2	$0.01 \leq N_T \leq 0.20$
Activation energy parameter	$E = \frac{E_A}{K_B T_\infty}$	1	$0.4 \leq E \leq 1.0$
Brownian motion parameter	$N_B = \frac{(\rho C_p)_{np} D_B \chi_\infty}{(\rho C_p) \nu \delta_\chi}$	0.1	$0.1 \leq N_B \leq 0.3$
Schmidt number	$Sc = \frac{\nu}{D_B}$	1	$1 \leq Sc \leq 3$

These conservation equations are governed by the following BCs:

$$BC_{s(u,v,p)}: \left\{ \begin{aligned} u(r, z = 0) = 0, v(r, z = 0) = \Omega r, w(r, z = 0) = 0, \\ u(r, z \rightarrow \infty) \rightarrow 0, v(r, z \rightarrow \infty) \rightarrow 0, p(r, z \rightarrow \infty) \rightarrow p_{\infty} \end{aligned} \right\}, \quad (7)$$

$$BC_{sT}: \left\{ \begin{aligned} \frac{\partial T}{\partial z}(r, z = 0) = \frac{h_f}{\kappa} [T(r, z = 0) - T_f], T(r, z \rightarrow \infty) \rightarrow T_{\infty} \end{aligned} \right\}, \quad (8)$$

$$BC_{s\chi}: \left\{ \frac{\partial \chi}{\partial z}(r, z = 0) = -\frac{\delta_{\chi} D_T}{D_B T_{\infty}} \frac{\partial T}{\partial z}(r, z = 0), \chi(r, z \rightarrow \infty) \rightarrow \chi_{\infty} \right\}. \quad (9)$$

For the sake of brevity, the meanings of the physical symbols and abbreviations used above are well regrouped in the nomenclature table. Further, it is preferable to introduce feasible similarity alterations into Eqs. 1–9 as suggested below:

$$\left\{ \begin{aligned} \xi = \sqrt{\frac{\Omega}{\nu}} z, F(\xi) = \frac{u}{\Omega r}, G(\xi) = \frac{v}{\Omega r}, H(\xi) = \frac{w}{\sqrt{\Omega \nu}}, P(\xi) \\ = \frac{p - p_{\infty}}{\rho \nu \Omega}, \Theta(\xi) = \frac{T - T_{\infty}}{T_f - T_{\infty}}, C(\xi) = \frac{\chi - \chi_{\infty}}{\chi_{\infty}} \end{aligned} \right\}. \quad (10)$$

Accordingly, the following ODEs and BCs are yielded:

$$H'(\xi) + 2F(\xi) = 0, \quad (11)$$

$$F''(\xi) + G^2(\xi) - F^2(\xi) - F'(\xi)H(\xi) = 0, \quad (12)$$

$$G''(\xi) - MG(\xi) - 2F(\xi)G(\xi) - G'(\xi)H(\xi) = 0, \quad (13)$$

$$P'(\xi) - H''(\xi) + MH(\xi) + H(\xi)H'(\xi) = 0, \quad (14)$$

$$\Theta''(\xi) + \text{Pr}N_T \Theta'^2(\xi) + \text{Pr}N_B \Theta'(\xi)C'(\xi) - \text{Pr}H(\xi)\Theta'(\xi) + Q_E e^{-\delta\xi} = 0, \quad (15)$$

$$C''(\xi) + \frac{N_T}{N_B} \Theta''(\xi) - \text{Sc}H(\xi)C'(\xi) - \Gamma \text{Sc}[1 + \omega\Theta(\xi)]^n C(\xi) e^{\frac{-\xi}{1+\omega\Theta(\xi)}} = 0, \quad (16)$$

$$F(\xi = 0) = 0, G(\xi = 0) = 1, H(\xi = 0) = 0, \Theta'(\xi = 0) - \text{Bi}\Theta(\xi = 0)$$

$$= -\text{Bi}, C'(\xi = 0) = -\frac{N_T}{N_B} \Theta'(\xi = 0), \quad (17)$$

$$F(\xi \rightarrow \xi_{\infty}) \rightarrow 0, G(\xi \rightarrow \xi_{\infty}) \rightarrow 0, P(\xi \rightarrow \xi_{\infty}) \rightarrow 0,$$

$$\Theta(\xi \rightarrow \xi_{\infty}) \rightarrow 0, C(\xi \rightarrow \xi_{\infty}) \rightarrow 0. \quad (18)$$

For more clarification on the influencing parameters involved in Eqs. 13–17, a technical list of the pertinent flow parameters is provided properly as seen in Table 1.

Fundamentally, the total viscous frictional coefficient  $C_{fr}$  and the thermal transfer rate  $Nu_r$  featuring hydrothermally the present nanofluid flow are defined locally by:

$$C_{fr} = \frac{\sqrt{\tau_{wr}^2 + \tau_{w\phi}^2}}{\rho(\Omega r)^2}, \quad (19)$$

$$Nu_r = \frac{r q_T}{k(T_f - T_{\infty})}. \quad (20)$$

Besides, the wall shear stress components ( $\tau_{wr}, \tau_{w\phi}$ ) and the wall heat flux  $q_T$  are given by:

$$\tau_{wr} = \mu \left( \frac{\partial u}{\partial z} + \frac{\partial w}{\partial r} \right)_{z=0}, \quad (21)$$

$$\tau_{w\phi} = \mu \left( \frac{\partial v}{\partial z} + \frac{1}{r} \frac{\partial w}{\partial \phi} \right)_{z=0}, \quad (22)$$

$$q_T = -k \left( \frac{\partial T}{\partial z} \right)_{z=0}. \quad (23)$$

By injecting the transformations of Eq. 10 into Eqs. 19–23, we get the reduced forms :

$$C_f = \sqrt{F'^2(0) + G'^2(0)}, \quad (24)$$

$$Nu = -\Theta'(0). \quad (25)$$

As underlined above, the reduced quantities ( $C_f, Nu$ ) are given by:

$$C_f = \text{Re}_r^{\frac{1}{2}} C_{fr}, \quad (26)$$

$$Nu = \text{Re}_r^{\frac{1}{2}} Nu_r. \quad (27)$$

Before starting the numerical modeling of the present nanofluid flow problem, the spatial physical domain  $[0, \xi_{\infty}]$  should be altered to the computational domain  $[0, 1]$  by introducing another spatial variable  $\varsigma$  into the dimensionless functions  $\{F(\xi), G(\xi), H(\xi), P(\xi), \Theta(\xi), C(\xi)\}$  and their derivatives

$\{F^{(m)}(\xi), G^{(m)}(\xi), H^{(m)}(\xi), P^{(m)}(\xi), \Theta^{(m)}(\xi), C^{(m)}(\xi)\}$  as follows:

$$\left\{ \begin{aligned} \left[ \begin{matrix} F(\xi) \\ G(\xi) \\ H(\xi) \\ P(\xi) \\ \Theta(\xi) \\ C(\xi) \end{matrix} \right] = \left[ \begin{matrix} F(\xi_{\infty}\varsigma) \\ G(\xi_{\infty}\varsigma) \\ H(\xi_{\infty}\varsigma) \\ P(\xi_{\infty}\varsigma) \\ \Theta(\xi_{\infty}\varsigma) \\ C(\xi_{\infty}\varsigma) \end{matrix} \right] = \left[ \begin{matrix} \bar{F}(\varsigma) \\ \bar{G}(\varsigma) \\ \bar{H}(\varsigma) \\ \bar{P}(\varsigma) \\ \bar{\Theta}(\varsigma) \\ \bar{C}(\varsigma) \end{matrix} \right], \text{ where } \left[ \begin{matrix} F^{(m)}(\xi) \\ G^{(m)}(\xi) \\ H^{(m)}(\xi) \\ P^{(m)}(\xi) \\ \Theta^{(m)}(\xi) \\ C^{(m)}(\xi) \end{matrix} \right] \\ = \frac{1}{\xi_{\infty}^m} \left[ \begin{matrix} \bar{F}(\varsigma) \\ \bar{G}(\varsigma) \\ \bar{H}(\varsigma) \\ \bar{P}(\varsigma) \\ \bar{\Theta}(\varsigma) \\ \bar{C}(\varsigma) \end{matrix} \right] \text{ and } \varsigma = \frac{\xi}{\xi_{\infty}}. \end{aligned} \right. \quad (28)$$

By focussing only on the physical function  $\{F(\xi), G(\xi), H(\xi), \Theta(\xi), C(\xi)\}$  and adopting the transformation of Eq. 28, the following differential system is obtained:

$$\left. \begin{aligned}
 &\bar{F}(\zeta) = 0, \text{ when } \zeta = 0, \\
 &\frac{1}{\xi_\infty^2} \bar{F}''(\zeta) + \bar{G}^2(\zeta) - \bar{F}^2(\zeta) - \frac{1}{\xi_\infty} \bar{H}(\zeta) \bar{F}'(\zeta) = 0, \text{ when } \zeta \neq 0, 1, \\
 &\bar{F}(\zeta) \rightarrow 0, \text{ when } \zeta \rightarrow 1, \\
 &\bar{G}(\zeta) - 1 = 0, \text{ when } \zeta = 0, \\
 &\frac{1}{\xi_\infty^2} \bar{G}''(\zeta) - M \bar{G}(\zeta) - 2 \bar{F}(\zeta) \bar{G}(\zeta) - \frac{1}{\xi_\infty} \bar{H}(\zeta) \bar{G}'(\zeta) = 0, \text{ when } \zeta \neq 0, 1, \\
 &\bar{G}(\zeta) \rightarrow 0, \text{ when } \zeta \rightarrow 1, \\
 &\bar{H}(\zeta) = 0, \text{ when } \zeta = 0, \\
 &\frac{1}{\xi_\infty} \bar{H}'(\zeta) + 2 \bar{F}(\zeta) = 0, \text{ when } \zeta \neq 0, \\
 &\frac{1}{\xi_\infty} \bar{\Theta}'(\zeta) - Bi \bar{\Theta}(\zeta) + Bi = 0, \text{ when } \zeta = 0, \\
 &\frac{1}{\xi_\infty^2} \bar{\Theta}''(\zeta) + \frac{Pr N_T}{\xi_\infty^2} \bar{\Theta}'(\zeta) + \frac{Pr N_B}{\xi_\infty^2} \bar{\Theta}'(\zeta) \bar{C}'(\zeta) \\
 &\quad - \frac{Pr}{\xi_\infty} \bar{H}(\zeta) \bar{\Theta}'(\zeta) + Q_E e^{-\delta \xi_\infty \zeta} = 0, \text{ when } \zeta \neq 0, 1, \\
 &\bar{\Theta}(\zeta) \rightarrow 0, \text{ when } \zeta \rightarrow 1, \\
 &\frac{1}{\xi_\infty} \bar{C}'(\zeta) = -\frac{N_T}{\xi_\infty N_B} \bar{\Theta}'(\zeta), \text{ when } \zeta = 0, \\
 &\frac{1}{\xi_\infty^2} \bar{C}''(\zeta) + \frac{N_T}{\xi_\infty^2 N_B} \bar{\Theta}''(\zeta) - \frac{Sc}{\xi_\infty} \bar{H}(\zeta) \bar{C}'(\zeta) - \Gamma Sc \left[ 1 + \omega \bar{\Theta}(\zeta) \right]^n \\
 &\bar{C}(\zeta) e^{\frac{\beta}{1+\omega \bar{\Theta}(\zeta)}} = 0, \text{ when } \zeta \neq 0, 1, \\
 &\bar{C}(\zeta) \rightarrow 0, \text{ when } \zeta \rightarrow 1
 \end{aligned} \right\} \tag{29}$$

Also, Eq. 24 and 25 are altered to:

$$C_f = \frac{1}{\xi_\infty} \sqrt{\bar{F}'^2(0) + \bar{G}'^2(0)}, \tag{30}$$

$$Nu = -\frac{1}{\xi_\infty} \bar{\Theta}'(0). \tag{31}$$

### 3 Numerical solution methodology

Numerically, the precise approximate solutions satisfying the nonlinear coupled differential system of Eq. 29 can be developed easily via an advanced hybrid algorithm GDQM-NRIT, which is principally based on the generalized differential quadrature method (GDQM) and Newton-Raphson’s iterative technique (NRIT). For this purpose, a non-uniform distribution of spatial collocation nodes  $\zeta_i$  along the reduced computational domain  $[\zeta_1, \zeta_N]$  is considered based on Gauss-Lobatto’s grid points, which are defined as:

$$\zeta_i = \frac{1}{2} - \frac{1}{2} \cos\left(\frac{\pi i - \pi}{N - 1}\right), \tag{32}$$

$$[\zeta_1, \zeta_N] = [0, 1] = \bigcup_{p=1}^{p=N-1} [\zeta_p, \zeta_{p+1}], \tag{33}$$

where  $1 \leq i \leq N$ .

In the framework of the proposed numerical procedure, the following generalized differential quadrature approximations are invoked during the  $\zeta$ -discretization of the resulting equations in the one-dimension Gauss-Lobatto space:

$$\bar{F}^{(m)}(\zeta_i) = \sum_{j=1}^N d_{ij}^{(m)} \bar{F}_j, \tag{34}$$

$$\bar{G}^{(m)}(\zeta_i) = \sum_{j=1}^N d_{ij}^{(m)} \bar{G}_j, \tag{35}$$

$$\bar{H}^{(m)}(\zeta_i) = \sum_{j=1}^N d_{ij}^{(m)} \bar{H}_j, \tag{36}$$

$$\bar{\Theta}^{(m)}(\zeta_i) = \sum_{j=1}^N d_{ij}^{(m)} \bar{\Theta}_j, \tag{37}$$

$$\bar{C}^{(m)}(\zeta_i) = \sum_{j=1}^N d_{ij}^{(m)} \bar{C}_j, \tag{38}$$

in which

$$\left\{ \bar{F}(\zeta_j) = \bar{F}_j, \bar{G}(\zeta_j) = \bar{G}_j, \bar{H}(\zeta_j) = \bar{H}_j, \bar{\Theta}(\zeta_j) = \bar{\Theta}_j, \bar{C}(\zeta_j) = \bar{C}_j \right\}. \tag{39}$$

Computationally, the mathematical algorithm of the weighing GDQ coefficients  $d_{ij}^{(m)}$  of Eqs. 34–38 is structured as follows:

$$\left. \begin{aligned}
 &d_{ij}^{(m)} = \frac{\prod_{p=1, p \neq i}^N (\zeta_i - \zeta_p)}{(\zeta_i - \zeta_j) \prod_{p=1, p \neq j}^N (\zeta_j - \zeta_p)}, \\
 &\text{for } m = 1, i \neq j, \text{ and } 1 \leq i, j \leq N, \text{ where } d_{ij}^{(1)} = Q_{ij}, \\
 &d_{ij}^{(m)} = m \left[ d_{ii}^{(m-1)} d_{ij}^{(1)} - \frac{d_{ij}^{(m-1)}}{(\zeta_i - \zeta_j)} \right], \\
 &\text{for } m > 1, i \neq j, \text{ and } 1 \leq i, j \leq N, \text{ where } d_{ij}^{(2)} = R_{ij}, \\
 &d_{ij}^{(m)} = - \sum_{p=1, p \neq i}^N d_{ip}^{(m)}, \text{ for } m \geq 1, i = j, \text{ and } 1 \leq i, j \leq N, \\
 &\text{where } \zeta_i = \frac{1}{2} - \frac{1}{2} \cos\left(\frac{\pi i - \pi}{N - 1}\right), \\
 &\zeta_j = \frac{1}{2} - \frac{1}{2} \cos\left(\frac{\pi j - \pi}{N - 1}\right), \text{ and } \zeta_p = \frac{1}{2} - \frac{1}{2} \cos\left(\frac{\pi p - \pi}{N - 1}\right)
 \end{aligned} \right\}. \tag{40}$$

Accordingly, we obtain the following nonlinear algebraic system:

$$\left. \begin{aligned}
 & \bar{F}_i = 0, \text{ when } i = 1, \\
 & \frac{1}{\xi_\infty^2} \sum_{j=1}^N R_{ij} \bar{F}_j + \bar{G}_i^2 - \bar{F}_i^2 - \frac{1}{\xi_\infty} \bar{H}_i \sum_{j=1}^N Q_{ij} \bar{F}_j = 0, \text{ when } i \neq 1, N, \\
 & \bar{F}_i \rightarrow 0, \text{ when } i = N, \\
 & \bar{G}_i - 1 = 0, \text{ when } i = 1, \\
 & \frac{1}{\xi_\infty^2} \sum_{j=1}^N R_{ij} \bar{G}_j - M \bar{G}_i - 2 \bar{F}_i \bar{G}_i - \frac{1}{\xi_\infty} \bar{H}_i \sum_{j=1}^N Q_{ij} \bar{G}_j = 0, \text{ when } i \neq 1, N, \\
 & \bar{G}_i \rightarrow 0, \text{ when } i = N, \\
 & \bar{H}_i = 0, \text{ when } i = 1, \\
 & \frac{1}{\xi_\infty} \sum_{j=1}^N Q_{ij} \bar{H}_j + 2 \bar{F}_i = 0, \text{ when } i \neq 1, \\
 & \frac{1}{\xi_\infty} \sum_{j=1}^N Q_{ij} \bar{\Theta}_j - Bi \bar{\Theta}_i + Bi = 0, \text{ when } i = 1, \\
 & \frac{1}{\xi_\infty^2} \sum_{j=1}^N R_{ij} \bar{\Theta}_j + \frac{Pr N_T}{\xi_\infty^2} \left( \sum_{j=1}^N Q_{ij} \bar{\Theta}_j \right)^2 + \frac{Pr N_B}{\xi_\infty^2} \sum_{j=1}^N Q_{ij} \bar{\Theta}_j \sum_{j=1}^N Q_{ij} \bar{C}_j \\
 & - \frac{Pr}{\xi_\infty} \bar{H}_i \sum_{j=1}^N Q_{ij} \bar{\Theta}_j + Q_E e^{-\delta \xi_\infty \zeta_i} = 0, \text{ when } i \neq 1, N, \\
 & \bar{\Theta}_i \rightarrow 0, \text{ when } i = N, \\
 & \frac{1}{\xi_\infty} \sum_{j=1}^N Q_{ij} \bar{C}_j = -\frac{N_T}{\xi_\infty N_B} \sum_{j=1}^N Q_{ij} \bar{\Theta}_j, \text{ when } i = 1, \\
 & \frac{1}{\xi_\infty^2} \sum_{j=1}^N R_{ij} \bar{C}_j + \frac{N_T}{\xi_\infty^2 N_B} \sum_{j=1}^N R_{ij} \bar{\Theta}_j - \frac{Sc}{\xi_\infty} \bar{H}_i \sum_{j=1}^N Q_{ij} \bar{C}_j - \Gamma Sc (1 + \omega \bar{\Theta}_i)^n \\
 & \bar{C}_i e^{\frac{-E}{1+\omega \bar{\Theta}_i}} = 0, \text{ when } i \neq 1, N, \\
 & \bar{C}_i \rightarrow 0, \text{ when } i = N
 \end{aligned} \right\} \quad (41)$$

An efficient NRIT algorithm has been developed properly to generate accurate discrete solutions  $\{(\bar{F}_i, \bar{G}_i, \bar{H}_i, \bar{\Theta}_i, \bar{C}_i), \text{ where } 1 \leq i \leq N\}$  for the above gigantic algebraic system with a higher order of exactitude. Sequel to this numerical treatment, the following square residual errors (SREs) are assessed numerically:

$$\Delta \bar{F} = \int_0^1 \left[ \frac{1}{\xi_\infty^2} \bar{F}''(\zeta) + \bar{G}^2(\zeta) - \bar{F}^2(\zeta) - \frac{1}{\xi_\infty} \bar{H}(\zeta) \bar{F}'(\zeta) \right]^2 d\zeta, \quad (42)$$

$$\Delta \bar{G} = \int_0^1 \left[ \frac{1}{\xi_\infty^2} \bar{G}''(\zeta) - M \bar{G}(\zeta) - 2 \bar{F}(\zeta) \bar{G}(\zeta) - \frac{1}{\xi_\infty} \bar{H}(\zeta) \bar{G}'(\zeta) \right]^2 d\zeta, \quad (43)$$

$$\Delta \bar{H} = \int_0^1 \left[ \frac{1}{\xi_\infty} \bar{H}'(\zeta) + 2 \bar{F}(\zeta) \right]^2 d\zeta, \quad (44)$$

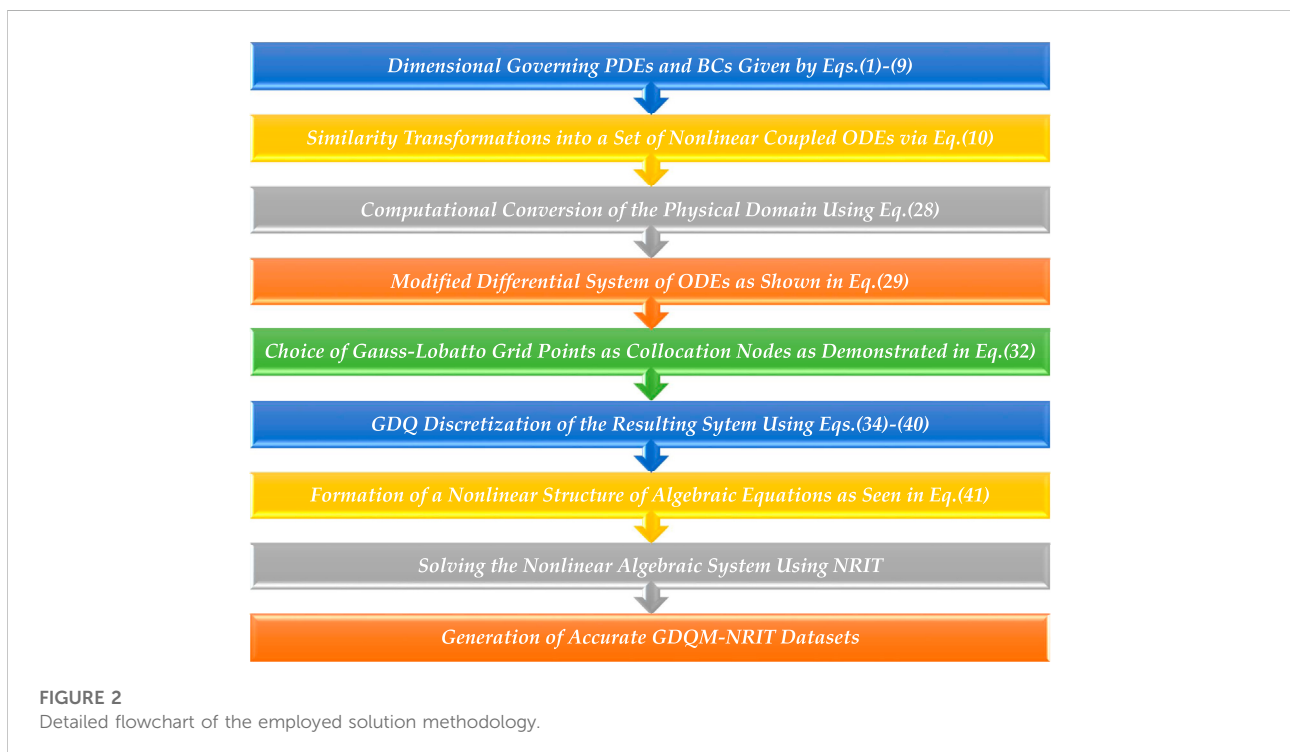
$$\Delta \bar{\Theta} = \int_0^1 \left[ \frac{1}{\xi_\infty^2} \bar{\Theta}''(\zeta) + \frac{Pr N_T}{\xi_\infty^2} \bar{\Theta}'^2(\zeta) + \frac{Pr N_B}{\xi_\infty^2} \bar{\Theta}'(\zeta) \bar{C}'(\zeta) - \frac{Pr}{\xi_\infty} \bar{H}(\zeta) \bar{\Theta}'(\zeta) + Q_E e^{-\delta \xi_\infty \zeta} \right]^2 d\zeta, \quad (45)$$

$$\Delta \bar{C} = \int_0^1 \left[ \frac{1}{\xi_\infty^2} \bar{C}''(\zeta) + \frac{N_T}{N_B \xi_\infty^2} \bar{\Theta}'(\zeta) - \frac{Sc}{\xi_\infty} \bar{H}(\zeta) \bar{C}'(\zeta) - \Gamma Sc [1 + \omega \bar{\Theta}(\zeta)]^n \bar{C}(\zeta) e^{\frac{-E}{1+\omega \bar{\Theta}(\zeta)}} \right]^2 d\zeta, \quad (46)$$

Briefly, the most important strategic steps involved in the suggested methodological solution are outlined in Figure 2.

Once the computed SREs reach very low values, the following dimensionless physical quantities can be deduced accurately:

$$\left. \begin{aligned}
 & F(\xi_i) = \bar{F}(\zeta_i), \text{ where } 1 \leq i \leq N \text{ and } \xi = \xi_\infty \zeta, \\
 & G(\xi_i) = \bar{G}(\zeta_i), \text{ where } 1 \leq i \leq N \text{ and } \xi = \xi_\infty \zeta, \\
 & H(\xi_i) = \bar{H}(\zeta_i), \text{ where } 1 \leq i \leq N \text{ and } \xi = \xi_\infty \zeta, \\
 & \Theta(\xi_i) = \bar{\Theta}(\zeta_i), \text{ where } 1 \leq i \leq N \text{ and } \xi = \xi_\infty \zeta, \\
 & C(\xi_i) = \bar{C}(\zeta_i), \text{ where } 1 \leq i \leq N \text{ and } \xi = \xi_\infty \zeta
 \end{aligned} \right\}, \quad (47)$$



$$F'(0) = \frac{1}{\xi_\infty} \sum_{j=1}^N Q_{1j} \bar{F}_j, \tag{48}$$

$$G'(0) = \frac{1}{\xi_\infty} \sum_{j=1}^N Q_{1j} \bar{G}_j, \tag{49}$$

$$H(\infty) = \bar{H}(\zeta_N) \tag{50}$$

$$C_f = \frac{1}{\xi_\infty} \sqrt{\left(\sum_{j=1}^N Q_{1j} \bar{F}_j\right)^2 + \left(\sum_{j=1}^N Q_{1j} \bar{G}_j\right)^2}, \tag{51}$$

$$\Theta(0) = \bar{\Theta}(\zeta_1), \tag{52}$$

$$\Theta'(0) = \frac{1}{\xi_\infty} \sum_{j=1}^N Q_{1j} \bar{\Theta}_j, \tag{53}$$

$$Nu = -\frac{1}{\xi_\infty} \sum_{j=1}^N Q_{1j} \bar{\Theta}_j, \tag{54}$$

$$C^*(0) = \frac{\chi_w}{\chi_\infty} = \bar{C}(\zeta_1) + 1, \tag{55}$$

$$C'(0) = \frac{1}{\xi_\infty} \sum_{j=1}^N Q_{1j} \bar{C}_j. \tag{56}$$

### 4 Multiple validations of generalized differential quadrature method-Newton-Raphson's iterative technique results

A perfect authentication of the executed GDQM-NRIT code has been demonstrated evidently in Table 2 for the quantities  $\{F'(0), G'(0), H(\infty), \Theta'(0)\}$  by comparing the computed GDQM-NRIT values with those estimated by previously Turkiymazoglu [27] in a certain special case study using the semi-analytical ESAT procedure. As anticipated, the extensive comparative tests performed quantitatively between the results of GDQM-NRIT and ESAT reflect forcefully the correctness of our outputted GDQM-NRIT outcomes, which are evaluated accordingly with very small square residual errors  $\{\Delta F, \Delta G, \Delta H, \Delta \Theta\}$ . To check again the correctness of the present GDQM-NRIT numerical simulation, a general corroboration has been

carried out for the studied nanofluid flow problem as shown in Table 3 by examining the accurateness order of the results given by the proposed GDQM-NRIT algorithm to those outputted additionally *via* another most commonly used method based on an efficient RKFM-ST numerical subroutine. Quantitatively, it is found an outstanding agreement between the results of GDQM-NRIT and RKFM-ST. Thus, the prime preliminary emphasized objectives of the present investigation can be accessed accurately *via* the developed GDQM-NRIT code. Furthermore, it is worth noting here that all the tabular results are provided with an absolute accuracy level of the order of  $10^{-10}$ .

### 5 Results and discussion

This illustrative section is dedicated especially to the physical deliberations of MHD Von Kármán's flow that can be happened suddenly within a chemically reactive nanofluidic medium in the presence of an internal heat generation. In this respect, several physical aspects have been explored for this kind of axisymmetric flow under the significant impact of a radial magnetic source. To strengthen the onset of heat and mass transport phenomena within the nanofluidic medium, a chemical reaction mechanism is taken place destructively according to Arrhenius's kinetics and the thermal aid of an exponentially decaying space-dependent heat generation source, in the case where the disk surface is heated convectively and unaffected by the vertical nanoparticles' mass flux. Based on the generated GDQM-NRIT outputs, numerous dimensionless demonstrations are portrayed properly for the radial, azimuthal, and transverse velocity fields  $\{F(\xi), G(\xi), H(\xi)\}$ , the nanofluid temperature and nanoparticles' molar concentration profiles  $\{\Theta(\xi), C(\xi)\}$ , the local frictional and heat transfer rate factors  $\{C_f, Nu\}$ , as well as the wall characteristics  $\{\Theta(0), C^*(0)\}$  as revealed graphically and tabularly in Figures 3–15, Table 4 and Table 5. To provide noticeably comparable graphical upshots, the curves of Figures 3–15 are plotted skilfully *via* professional graphical tools (e.g., Grapher and Surfer) to evidence the responses of dimensionless quantities  $\{F(\xi), G(\xi), H(\xi), \Theta(\xi), C(\xi), C^*(0)\}$  against the mounting parametric values of  $M$ -Magnetic parameter,

TABLE 2 Comparison between the results of GDQM-NRIT and ESAT.

$\{M = 0.5, Pr = 1, Bi \rightarrow \infty, Q_E = 0, N_T = 0, Sc = 0, \Gamma = 0, \xi_\infty = 10, N = 70\}$

ESAT [27]	GDQM-NRIT	
$F'(0) = 0.426484$	$F'(0) = 0.4264843113$	$\Delta F = 5.87 \times 10^{-21}$
$G'(0) = -0.877127$	$G'(0) = -0.8771269589$	$\Delta G = 2.58 \times 10^{-28}$
$H(\infty) = -0.706957$	$H(\infty) = -0.7069566789$	$\Delta H = 8.34 \times 10^{-31}$
$\Theta'(0) = -0.340652$	$\Theta'(0) = -0.3406523300$	$\Delta \Theta = 8.21 \times 10^{-22}$

TABLE 3 General validation of GDQM- NRIT algorithm via RKFM-ST results.

{Pr = 3,  $\delta$  = 1,  $n$  = 0.5,  $\gamma$  = 0.2,  $\Gamma$  = 1,  $Bi$  = 5,  $N_T$  = 0.2,  $E$  = 1,  $N_B$  = 0.1,  $Sc$  = 1,  $N$  = 70}

First general validation when { $M$ = 0.01, $Q_E$ = 0.02, $\xi_{\infty}$ = 10}		
RKFM-ST	GDQM-NRIT	
Computed Quantities	Computed Quantities	SREs
$C_f$ = 0.8028876130	$C_f$ = 0.8028876130	$\Delta F + \Delta G = 2.16 \times 10^{-25}$
$H(\infty)$ = -0.8774401157	$H(\infty)$ = -0.8774401157	$\Delta H = 1.38 \times 10^{-29}$
$Nu$ = 0.5631294489	$Nu$ = 0.5631294489	$\Delta \Theta = 1.51 \times 10^{-24}$
$\Theta(0)$ = 0.8873741102	$\Theta(0)$ = 0.8873741102	
$C'(0)$ = 1.1262588978	$C'(0)$ = 1.1262588978	$\Delta C = 2.38 \times 10^{-25}$
$C^*(0)$ = 0.0758731236	$C^*(0)$ = 0.0758731236	
Second general validation when { $M$ = 1, $Q_E$ = 0.1, $\xi_{\infty}$ = 5}		
RKFM-ST	GDQM-NRIT	
Computed Quantities	Computed Quantities	SREs
$C_f$ = 1.1568993204	$C_f$ = 1.1568993204	$\Delta F + \Delta G = 3.49 \times 10^{-25}$
$H(\infty)$ = -0.4921398969	$H(\infty)$ = -0.4921398969	$\Delta H = 2.54 \times 10^{-30}$
$Nu$ = 0.3963842717	$Nu$ = 0.3963842717	$\Delta \Theta = 5.06 \times 10^{-23}$
$\Theta(0)$ = 0.9207231456	$\Theta(0)$ = 0.9207231456	
$C'(0)$ = 0.7927685434	$C'(0)$ = 0.7927685434	$\Delta C = 1.12 \times 10^{-24}$
$C^*(0)$ = 0.1689770814	$C^*(0)$ = 0.1689770814	

TABLE 4 Numerical estimation of frictional factor  $C_f$ .

M	{Pr = 3, $\delta$ = 1, $n$ = 0.5, $\gamma$ = 0.2, $\Gamma$ = 1, $\xi_{\infty}$ = 10, $N$ = 70}		
	$C_f$	$\Delta F$	$\Delta G$
1	1.1586320415	$3.74 \times 10^{-29}$	$1.41 \times 10^{-25}$
2	1.4922475645	$1.70 \times 10^{-29}$	$3.65 \times 10^{-26}$
3	1.7798987776	$1.45 \times 10^{-29}$	$1.00 \times 10^{-25}$

$Q_E$ –Heat generation parameter,  $Bi$ –Thermal Biot number,  $N_T$ –Thermophoresis parameter,  $E$ –Activation energy parameter,  $N_B$ –Brownian motion parameter, and  $Sc$ –Schmidt number by varying one of these parameters and keeping the others fixed at their default values underlined in Table 1.

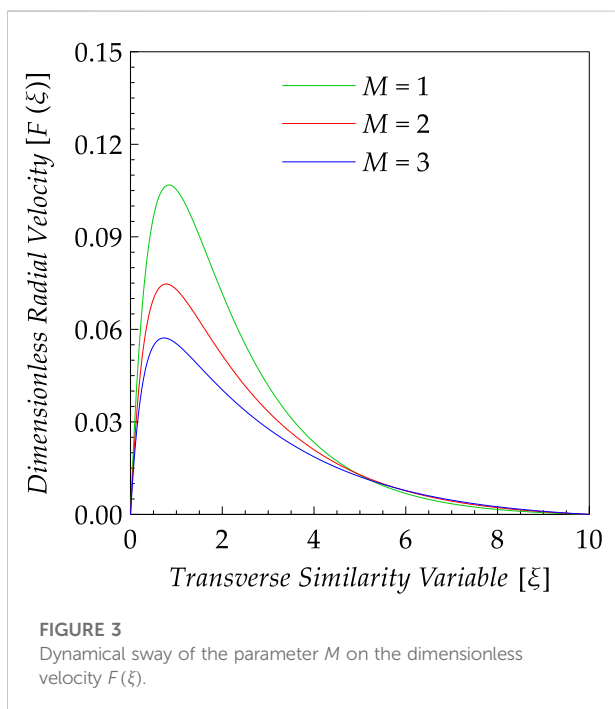
The unified dynamical influence of the magnetic parameter  $M$  on the dimensionless profiles  $\{F(\xi), G(\xi), -H(\xi)\}$  is clearly shown in Figures 3–5. Graphically, it is demonstrated from Figure 3 that the intense radial motion is seen near the rotating disk. Also, it is noticed from Figures 3–5 that the strengthening values of the magnetic parameter  $M$  create a considerable decline in the profiles  $\{F(\xi), G(\xi), -H(\xi)\}$ , which leads to an extensive

overall opposition to the nanofluid motion in the  $(r, \phi, -z)$ –directions. This fact can be explicated by the resistive influence of Lorentz’s forces, which are induced magnetically within the electrically conducting nanofluidic medium as a consequence of the physical interaction between the radially exerted magnetic field and the nanofluid motion.

Keeping in mind the hindering mechanical demeanor of Lorentz’s forces towards the nanofluid motion, an amount of thermal energy is communicated substantially. For this reason, the temperature profile  $\Theta(\xi)$  heightens with the elevating values of the magnetic parameter  $M$  as witnessed in Figure 6. From an energetical point of view, the

TABLE 5 Numerical estimation of thermal wall characteristics.

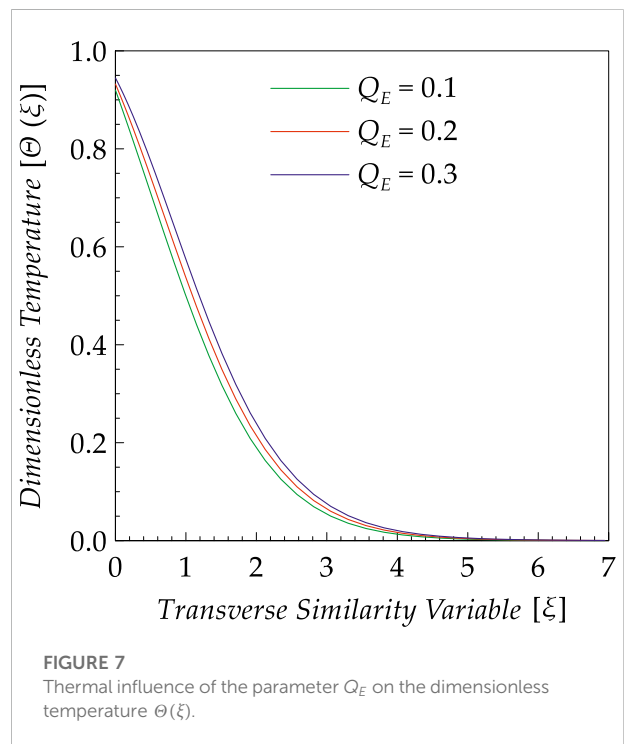
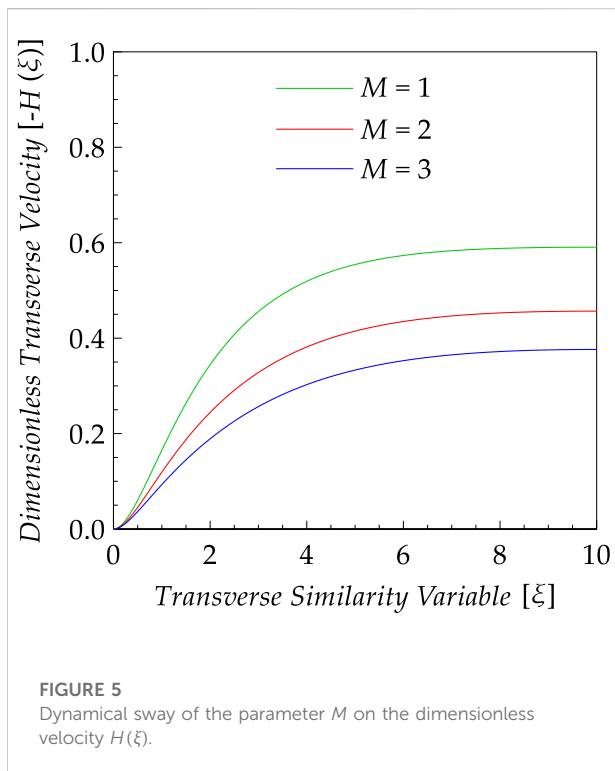
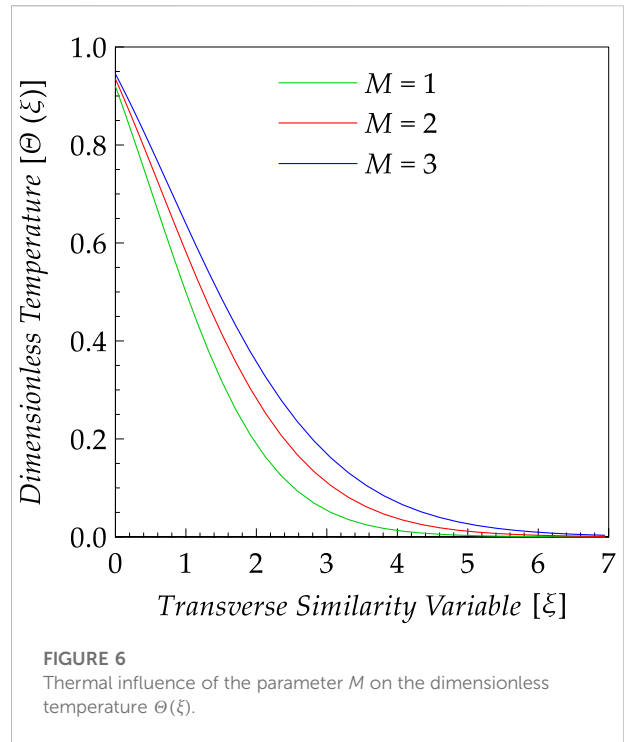
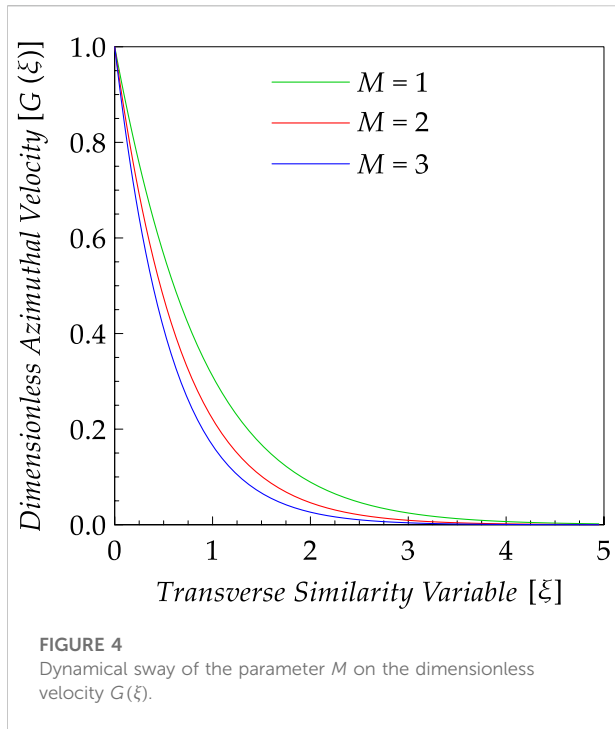
Parameters	Values	{Pr = 3, $\delta = 1, n = 0.5, \gamma = 0.2, \Gamma = 1, \xi_{\infty} = 10, N = 70$ }		
		Nu	$\Theta(0)$	$\Delta\Theta$
M	1	0.4010871118	0.9197825776	$4.24 \times 10^{-25}$
	2	0.3265024801	0.9346995039	$1.45 \times 10^{-22}$
	3	0.2753756861	0.9449248627	$1.73 \times 10^{-23}$
Q <sub>E</sub>	0.1	0.4010871118	0.9197825776	$4.24 \times 10^{-25}$
	0.2	0.3387469545	0.9322506091	$3.31 \times 10^{-25}$
	0.3	0.2762984863	0.9447403027	$1.80 \times 10^{-25}$
Bi	1	0.2967085471	0.7032914528	$2.45 \times 10^{-24}$
	2	0.3547316429	0.8226341785	$1.95 \times 10^{-23}$
	5	0.4010871118	0.9197825776	$4.24 \times 10^{-25}$
N <sub>T</sub>	0.01	0.4284091396	0.9143181720	$1.14 \times 10^{-23}$
	0.10	0.4155276538	0.9168944692	$2.59 \times 10^{-25}$
	0.20	0.4010871118	0.9197825776	$4.24 \times 10^{-25}$
Sc	1	0.4010871118	0.9197825776	$4.24 \times 10^{-25}$
	2	0.3891965649	0.9221606870	$7.84 \times 10^{-26}$
	3	0.3818198866	0.9236360226	$1.61 \times 10^{-25}$
E	0.4	0.3930789236	0.9213842152	$8.20 \times 10^{-25}$
	0.7	0.3972549866	0.9205490026	$3.03 \times 10^{-25}$
	1.0	0.4010871118	0.9197825776	$4.24 \times 10^{-25}$



nanofluidic medium can be enhanced thermally more near the surface disk by the existence of a variable internal heat source exhibiting an exponentially decaying trend in the

$z$ -directions, whose potency can be controlled effectively through the heat generation parameter  $Q_E$ . Consequently, a sensitive upsurge in the temperature profile  $\Theta(\xi)$  is witnessed in Figure 7 as a response to the strengthening in the heat generation parameter  $Q_E$ . Similarly, the salient results of Figure 8 and Figure 9 prove the possibility of accomplishing an extra improvement in the temperature profile  $\Theta(\xi)$  via the higher estimation in the magnitudes of the thermal Biot number  $Bi$  and the thermophoresis parameter  $N_T$ . These valuable observations confirm that the heat transfer mechanism can be ameliorated within the nanofluidic medium either by diminishing the thermal resistance between the hot working fluid and the surface contact of the disk or by reinforcing the upward thermomigration of nanoparticles from the hot region to the cold zone.

In the framework of the passive control approach, the vertical nanoparticles' mass flux becomes zero at the surface disk due to its impermeability characteristic. In this case, Sherwood's number gets vanished as long as there is no mass transfer manifestation to evaluate quantitatively for the solid nanoparticles at the horizontal boundary. This physical situation leads to a top-heavy configuration, in which the solid nanoparticles will regroup more nearby the cold region as revealed in Figures 10–14 for the nanoparticles' molar concentration distribution  $C(\xi)$ . In the light of the present



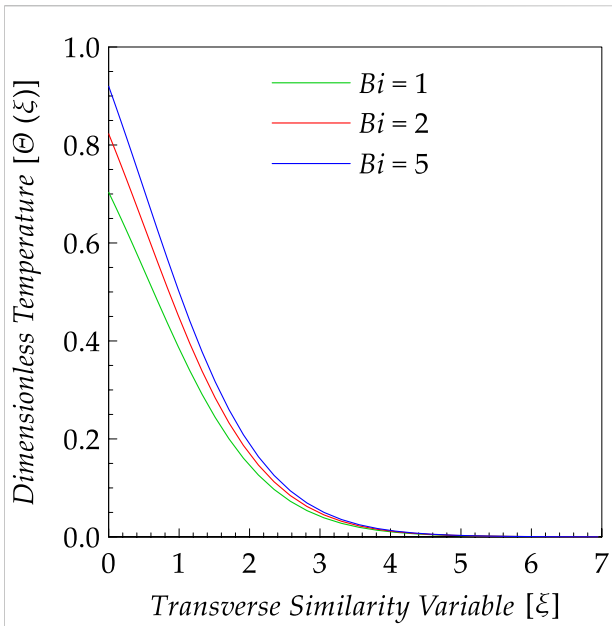


**FIGURE 8**  
Thermal influence of the parameter  $Bi$  on the dimensionless temperature  $\Theta(\xi)$ .

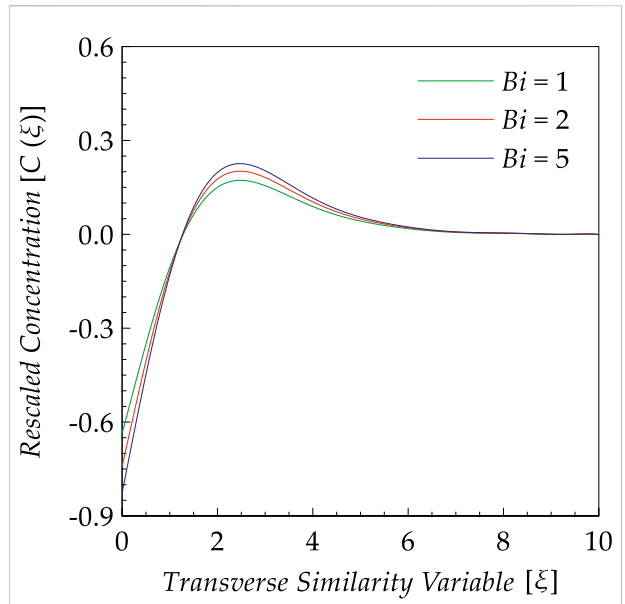


**FIGURE 10**  
Mass transportation impact of the parameter  $Bi$  on the rescaled concentration  $C(\xi)$ .

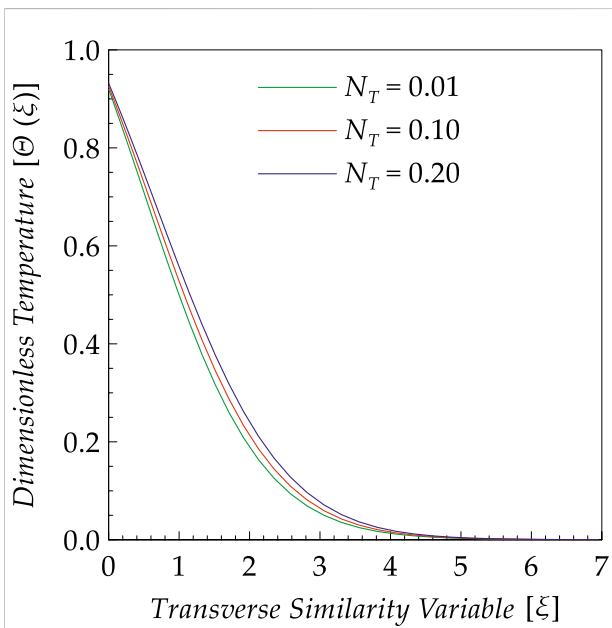


**FIGURE 9**  
Thermal influence of the parameter  $N_T$  on the dimensionless temperature  $\Theta(\xi)$ .

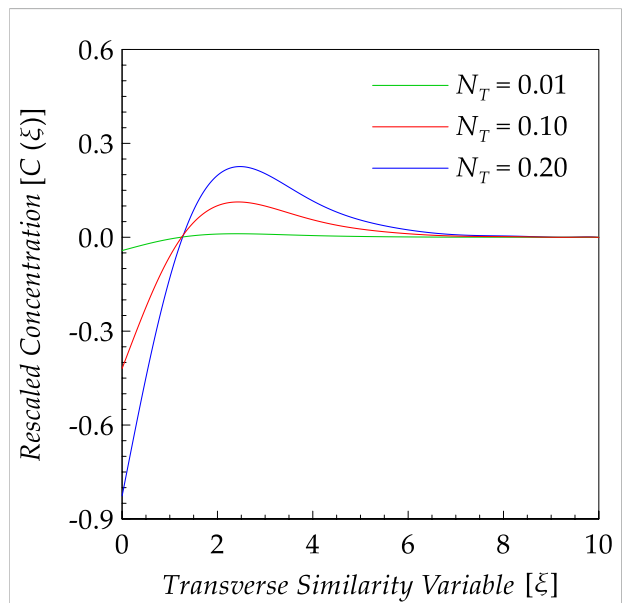
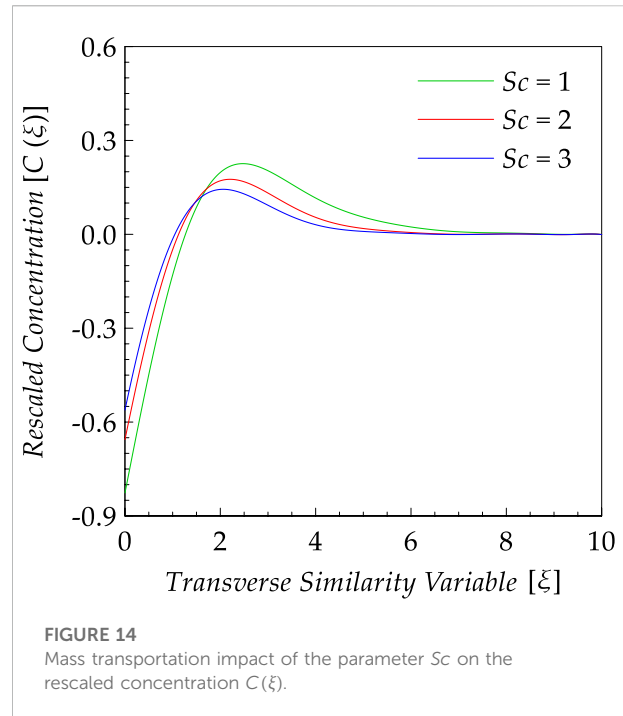
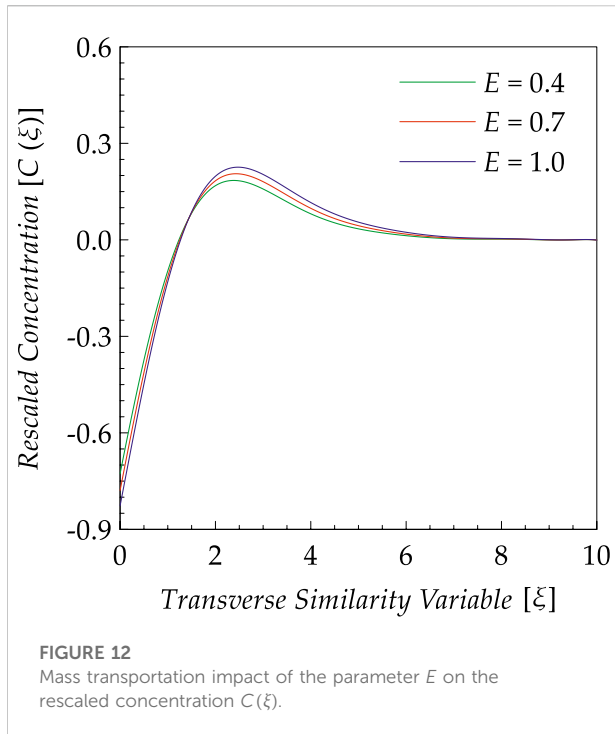
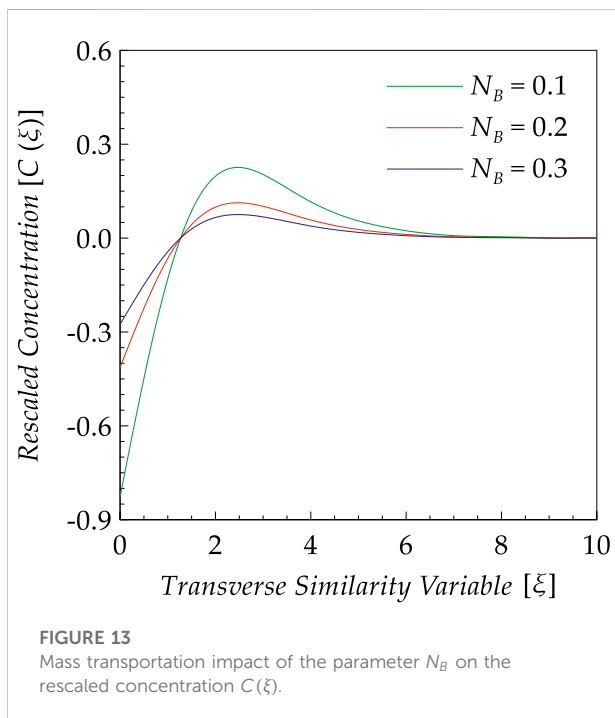


**FIGURE 11**  
Mass transportation impact of the parameter  $N_T$  on the rescaled concentration  $C(\xi)$ .



nanofluid flow model, it is confirmed in Figures 10–12 that the superior values of the thermal Biot number  $Bi$ , the thermophoresis parameter  $N_T$ , and the activation energy



parameter  $E$  can intensify the role of the thermophoretic forces by reinforcing the partial migration of nanoparticles from the disk surface (i.e., the hot region) to the surrounding region of the free-stream zone (i.e., the cold region), which leads to an important decay in the wall nanoparticles' molar concentration with a thickening in the concentration boundary layer region. On the other hand, the downward vertical motion of nanoparticles (i.e., the reciprocal migration of solid nanoparticles) can be accomplished within the nanofluidic medium by supporting the mass diffusive mechanism *via* the advanced values of the Brownian motion parameter  $N_B$  and the Schmidt number  $Sc$  as emphasized in Figure 13 and Figure 14. In this situation, an important escalation in the wall nanoparticles' molar concentration is obtained with a shrinking in the concentration boundary layer region. Moreover, the sways of the parameters  $\{Bi, N_T, E, N_B, Sc\}$  on the reduced wall concentration  $C^*(0)$  ascertained graphically in Figures 10–14 are accentuated in another way as witnessed in Figure 15.

From an engineering point of view, the behaviors of the reduced quantities  $\{C_f, Nu, \Theta(0)\}$  against the pertinent parameters are elucidated numerically in Table 4 and Table 5. It is important to mention that the surface drag force factor  $C_f$  can be reduced practically by diminishing the magnitude of the magnetic parameter  $M$ . However, an enhancement in the wall heat transfer rate  $Nu$  can be reached only *via* the growing values of the thermal Biot number  $Bi$  and the activation energy parameter  $E$ . Furthermore, it is found that the dimensionless wall

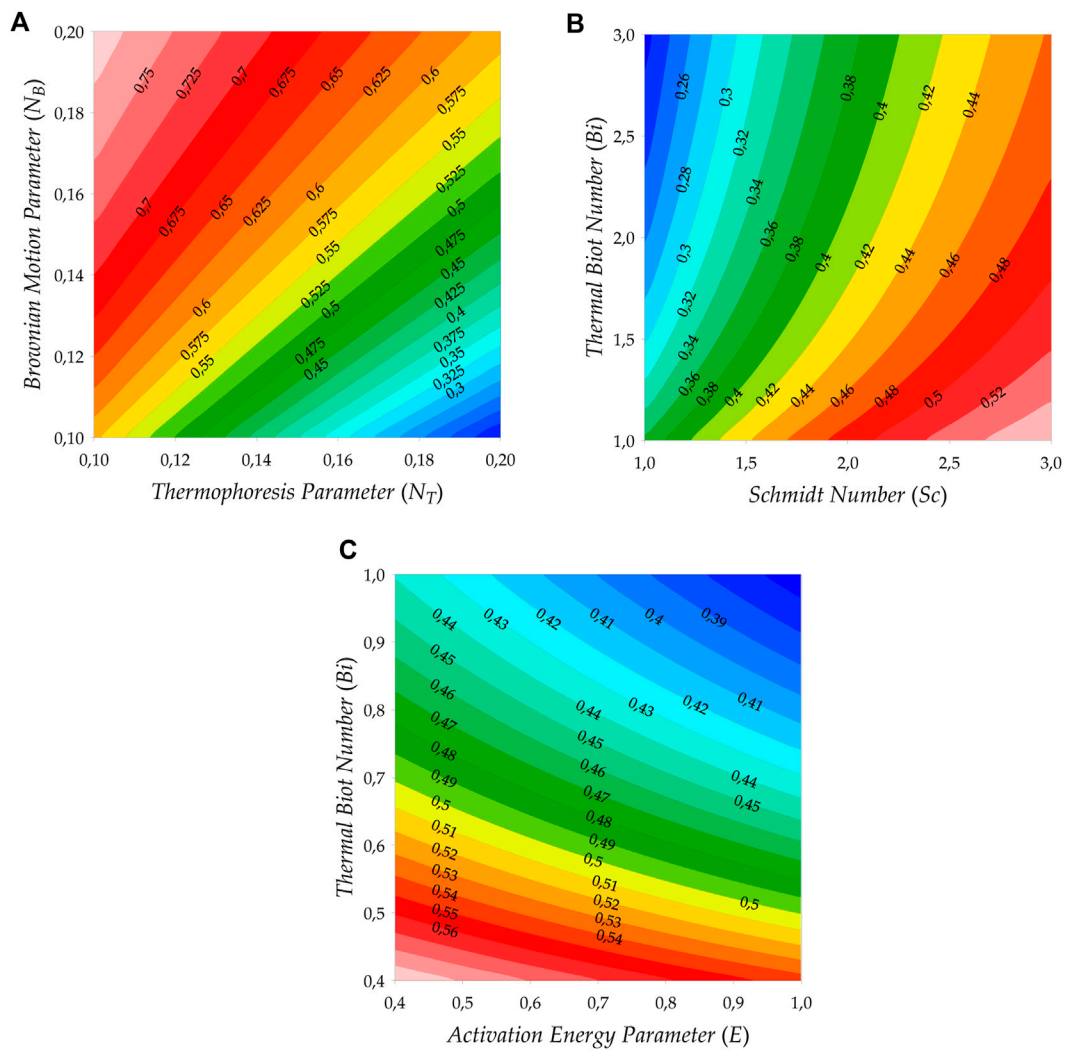


**FIGURE 15**  
Variation of dimensionless wall quantity  $C^*(0)$  against (A)  $N_T$  and  $N_B$ , (B)  $Sc$  and  $Bi$ , (C)  $E$  and  $Bi$ .

temperature  $\Theta(0)$  exhibits an elevating tendency in response to the mounting values of the parameters  $\{M, Q_E, Bi, N_T, Sc\}$ , whereas a reverse trend is observed for the activation energy parameter  $E$ .

## 6 Concluding remarks

Among the main derived remarks, we can write:

- The proposed numerical algorithm shows a higher degree of flexibility during the computational handling of the present nanofluid flow problem, in which the GDQM-NRIT results can be provided accurately with a low computational cost.

- A postponing effect is seen for the magnetic parameter towards the nanofluid motion in all directions.
- An elevation in the temperature profile can be achieved *via* the greater values of the magnetic parameter, the heat generation parameter, the thermal Biot number, and the thermophoresis parameter.
- A significant strengthening in the thermo-migration of nanoparticles can be obtained *via* the grander magnitudes of the thermal Biot number, the thermophoresis parameter, and the activation energy parameter.
- The downward motion of nanoparticles can be reinforced considerably *via* the increasing values of the Brownian motion parameter and the Schmidt number.
- The surface drag force factor can be reduced by weakening the magnetic parameter.

- The magnitude of the temperature gradient can be ameliorated significantly at the wall *via* the growing values of the activation energy parameter and thermal Biot number.
- Compared to other control parameters, the activation energy parameter  $E$  has a declining impact on the wall temperature.

## Data availability statement

The original contributions presented in the study are included in the article/supplementary material, further inquiries can be directed to the corresponding author.

## Author contributions

Data curation; AW, AA, KG, BB, RK, PK, and AJ. Formal analysis; AW, AA, KG, BB, RK, PK, and AJ. Investigation; AW, AA, KG, BB, RK, PK, and AJ. Supervision; PK. All authors discussed the results, wrote, and commented on the manuscript at all stages. All authors have read and agreed to the published version of the manuscript.

## Funding

This research was funded by the Science, Research and Innovation Promotion Fund (Grant No: 2495051). The project is funded by National Research Council of Thailand (NRCT) (Grant No: N42A650183). The authors would like to thank the

## References

1. Buongiorno J, Venerus DC, Prabhat N, McKrell T, Townsend J, Christianson R, et al. A benchmark study on the thermal conductivity of nanofluids. *J Appl Phys* (2009) 106:094312. doi:10.1063/1.3245330
2. Bergman TL, Incropera FP, Lavine AS, Dewitt DP. *Introduction to heat transfer*. John Wiley & Sons (2011).
3. Angayarkanni SA, Philip J. Review on thermal properties of nanofluids : Recent Developments. *Adv Colloid Interf Sci*. (2015) 225:146–76. doi:10.1016/j.cis.2015.08.014
4. Choi SUS, Eastman JA. In: DA Siginer HP Wang, editors. *Enhancing conductivity of fluids with nanoparticles, Developments and applications of non-Newtonian flows*, 66. New York: Am. Soc. Mech. Eng. (1995). p. 99–105.
5. Koo J, Kleinstreuer C. A new thermal conductivity model for nanofluids. *J Nanopart Res* (2004) 6:577–88. doi:10.1007/s11051-004-3170-5
6. Koo J, Kleinstreuer C. Viscous dissipation effects in microtubes and microchannels. *Int J Heat Mass Transf* (2004) 47:3159–69. doi:10.1016/j.ijheatmasstransfer.2004.02.017
7. Koo J, Kleinstreuer C. Laminar nanofluid flow in microheat-sinks. *Int J Heat Mass Transf* (2005) 48:2652–61. doi:10.1016/j.ijheatmasstransfer.2005.01.029
8. Koo J, Kleinstreuer C. Impact analysis of nanoparticle motion mechanisms on the thermal conductivity of nanofluids. *Int Commun Heat Mass Transfer* (2005) 32:1111–8. doi:10.1016/j.icheatmasstransfer.2005.05.014
9. Li J. *Computational analysis of nanofluid flow in micro-channels with applications to micro-heat sinks and bio-MEMS*. Ph.D. Thesis.

Deanship of Scientific Research at Umm Al-Qura University for supporting this work by Grant Code:(22UQU4331317DSR50).

## Acknowledgments

The authors extend their appreciation to the Deanship of Scientific Research at King Khalid University for funding this work through Large Groups [grant number RGP.2/208/43]. The authors would like to thank the Deanship of Scientific Research at Umm Al-Qura University for supporting this work by Grant Code:(22UQU4331317DSR50).

## Conflict of interest

RK and PK are employed by Geo-Informatics and Space Technology Development Agency (GISTDA).

The remaining authors declare that the research was conducted in the absence of any commercial or financial relationships that could be construed as a potential conflict of interest

## Publisher's note

All claims expressed in this article are solely those of the authors and do not necessarily represent those of their affiliated organizations, or those of the publisher, the editors and the reviewers. Any product that may be evaluated in this article, or claim that may be made by its manufacturer, is not guaranteed or endorsed by the publisher.

Raleigh, NC, the United States, Raleigh, NC, United States: NC State University (2008).

10. Corcione M. Empirical correlating equations for predicting the effective thermal conductivity and dynamic viscosity of nanofluids. *Energy Convers Manag* (2011) 52:789–93. doi:10.1016/j.enconman.2010.06.072

11. Waqas H, Yasmin S, Althobaiti N, Bonyah E, Alshehri A, Shah Z. Evaluating the higher-order slip consequence in bioconvection nanofluid flow configured by a variable thick surface of disk. *J Nanomater* (2022) 2022: 1–13. doi:10.1155/2022/2766317

12. Shah Z, Ullah A, Musa A, Vrinceanu N, Ferrandiz Bou S, Iqbal S, et al. Entropy optimization and thermal behavior of a porous system with considering hybrid nanofluid. *Front Phys* (2022) 10:1–15. doi:10.3389/fphy.2022.929463

13. Maneengam A, Bouzennada T, Aissa A, Guedri K, Weera W, Younis O, et al. Numerical study of lid-driven hybrid nanofluid flow in a corrugated porous cavity in the presence of magnetic field. *Nanomaterials* (2022) 12:2390–17. doi:10.3390/nano12142390

14. Alshare A, Aissa A, Guedri K, Younis O, Fayz-Al-Asad M, Ali HM, et al. Hydrothermal and entropy investigation of nanofluid natural convection in a lid-driven cavity concentric with an elliptical cavity with a wavy boundary heated from below. *Nanomaterials* (2022) 12:1392–17. doi:10.3390/nano12091392

15. Liu C, Pan M, Zheng L, Ming C, Zhang X. Flow and heat transfer of Bingham plastic fluid over a rotating disk with variable thickness. *Z Für Naturforsch. A*. (2016) 71:1003–15. doi:10.1515/zna-2016-0218

16. Hussain Z. Unsteady MHD flow due to eccentric rotations of a porous disk and an oscillating fluid at infinity. *ZAMM - J Appl Math Mech/Z Angew Mathematik Mechanik* (2021) 101:e202000369. doi:10.1002/zamm.202000369
17. Rández X, Zaversky F, Astrain D. A novel active volumetric rotating disks solar receiver for concentrated solar power generation. *Appl Therm Eng* (2022) 206: 118114. doi:10.1016/j.applthermaleng.2022.118114
18. Von Kármán T. Über laminare und turbulente Reibung. *Z Angew Math Mech* (1921) 1:233–52. Von Kármán. doi:10.1002/zamm.19210010401
19. Ahmadpour A, Sadeghy K. Swirling flow of Bingham fluids above a rotating disk: An exact solution. *J Nonnewton Fluid Mech* (2013) 197:41–7. doi:10.1016/j.jnnfm.2013.03.001
20. Khan U., Khan W, Badruddin IA, Ghaffari A, Ali HM. Heat transfer in steady slip flow of tangent hyperbolic fluid over the lubricated surface of a stretchable rotatory disk. *Case Stud Therm Eng* (2021) 24:100825. doi:10.1016/j.csite.2020.100825
21. Waini I, Ishak A, Pop I. Multiple solutions of the unsteady hybrid nanofluid flow over a rotating disk with stability analysis. *Eur J Mech - B/Fluids* (2022) 94:121–7. doi:10.1016/j.euromechflu.2022.02.011
22. Kumar M, Mondal PK. Irreversibility analysis of hybrid nanofluid flow over a rotating disk: Effect of thermal radiation and magnetic field. *Colloids Surf A: Physicochemical Eng Aspects* (2022) 635:128077. doi:10.1016/j.colsurfa.2021.128077
23. Mandal S, Shit GC. Entropy analysis on unsteady MHD biviscosity nanofluid flow with convective heat transfer in a permeable radiative stretchable rotating disk. *Chin J Phys* (2021) 74:239–55. doi:10.1016/J.CJPH.2021.07.036
24. Magodora M, Mondal H, Motsa S, Sibanda P. Numerical studies on gold-water nanofluid flow with activation energy Past A rotating disk. *Int J Appl Comput Math* (2022) 8:41. doi:10.1007/s40819-022-01241-4
25. Buongiorno J. Convective transport in nanofluids. *J Heat Transfer* (2006) 128: 240–50. doi:10.1115/1.2150834
26. Latiff NA, Uddin MJ, Ismail AIM. Stefan blowing effect on bioconvective flow of nanofluid over a solid rotating stretchable disk. *Propulsion Power Res* (2016) 5: 267–78. doi:10.1016/j.jprr.2016.11.002
27. Turkyilmazoglu M. Flow and heat over a rotating disk subject to a uniform horizontal magnetic field. *Z Für Naturforsch. A. January* (2022) 77:329–37. doi:10.1515/zna-2021-0350

## Nomenclature

- $B$  Magnetic field strength, [ $kg s^{-2} A^{-1}$ ]  
 $C$  Rescaled molar concentration of nanoparticles, [-]  
 $(D_T, D_B)$  Thermal and mass diffusive coefficients, [ $m^2 s^{-1}$ ]  
 $E_A$  Activation energy, [ $J$ ]  
 $(F, G, H)$  Dimensionless velocity components, [-]  
 $h_f$  Convective heat transfer coefficient, [ $W m^{-2} K^{-1}$ ]  
 $K_B$  Boltzmann constant, [ $J K^{-1}$ ]  
 $K_\chi$  Chemical reaction rate constant, [ $s^{-1}$ ]  
 $n$  Fitted rate constant, [-]  
 $N$  Number of grid points  
 $p$  Pressure, [ $Pa$ ]  
 $p_\infty$  Pressure at the free-stream region, [ $Pa$ ]  
 $Q$  Heat source potency, [ $J m^{-3} s^{-1} K^{-1}$ ]  
 $T$  Temperature distribution, [ $K$ ]  
 $T_f$  Temperature of the heating fluid, [ $K$ ]  
 $T_w$  Wall temperature, [ $K$ ]  
 $T_\infty$  Temperature distribution at the free-stream region, [ $K$ ]  
 $(u, v, w)$  Velocity components, [ $m s^{-1}$ ]  
 $(r, \phi, z)$  Cylindrical coordinates, [ $m, rad, m$ ]

## Greek symbols

- $\chi$  Molar concentration distribution of nanoparticles, [ $mol m^{-3}$ ]  
 $\chi_w$  Molar concentration of nanoparticles at the wall, [ $mol m^{-3}$ ]  
 $\chi_\infty$  Molar concentration of nanoparticles at the free-stream region, [ $mol m^{-3}$ ]  
 $\delta$  Parameter featuring the decaying trend of the heat source, [-]  
 $\delta_\chi$  Corrective factor for the molar concentration scale, [ $mol m^{-3}$ ]  
 $\kappa$  Thermal conductivity, [ $W m^{-1} K^{-1}$ ]  
 $\nu$  Kinematic viscosity, [ $m^2 s^{-1}$ ]  
 $\Theta$  Dimensionless temperature, [-]  
 $\rho$  Nanofluid density, [ $kg m^{-3}$ ]  
 $(\rho C_p)$  Nanofluid heat capacitance, [ $J m^{-3} K^{-1}$ ]  
 $(\rho C_p)_{np}$  Nanoparticles' heat capacitance, [ $J m^{-3} K^{-1}$ ]  
 $\sigma$  Nanofluid electrical conductivity, [ $S m^{-1}$ ]  
 $\varsigma$  Reduced similarity variable, [-]  
 $\xi$  Similarity variable, [-]

- $\xi_\infty$  The approximate value of  $\xi$  when  $\xi$  tends to infinity, [-]  
 $\Omega$  Rotating velocity, [ $rad s^{-1}$ ]

## Abbreviations

- $Al_2O_3$  Alumina nanoparticles  
 $BCs$  Boundary conditions  
 $BCs_w$  Boundary conditions at the wall  
 $BCs_\infty$  Boundary conditions in the free-stream region  
 $CMC$  Carboxy methyl cellulose  
 $Cu$  Copper nanoparticles  
**ESAT** Exponential series approximation technique  
 $Fe_3O_4$  Magnetite nanoparticles  
**GFET** Galerkin finite element technique  
**GDQ** Generalized differential quadrature  
**GDQM** Generalized differential quadrature method  
 $H_2O$  Water  
 $MWCNT$  Multi-wall carbon nanotubes  
**MHD** Magnetohydrodynamics  
**NRIT** Newton-Raphson iterative technique  
**ODEs** Ordinary differential equations  
**PDEs** Partial differential equations  
**RKFM** Runge-Kutta-Fehlberg method  
**ST** Shooting technique  
**SREs** Square residual errors

## Subscripts

- $np$  Nanoparticles  
 $w$  Wall condition  
 $\infty$  Free-stream condition

## Superscripts

- ' First-order derivative w.r.t  $\xi$  or  $\varsigma$   
'' Second-order derivative w.r.t  $\xi$  or  $\varsigma$   
 $(m)$   $m^{th}$ -order derivative w.r.t  $\varsigma$